Advancements in Zinc Oxide (ZnO) thin films for photonic and optoelectronic applications: a focus on doping and annealing processes

Zokirjon Mirzajonov[1*], *Khusanboy* Sulaymonov[1], *Tokhir* Rakhmonov[1], *Fakhriddin* Yusupov[1], *Dadakhon* Khidirov[1], and *Jakhongir* Rakhimjonov[1]

[1]Fergana Polytechnic Institute, 150107, Fergana, Uzbekistan

Abstract. This study focuses on the potential of Zinc oxide (ZnO) as a versatile material for photonic and optoelectronic applications, owing to its direct wide bandgap (Eg ≈ 3.175 eV) and significant excitonic energy. ZnO, both in pure and doped forms, exhibits promise in various domains, including solar cells, photoelectrochemical cells, thin film transistors, gas sensors, and nanogenerators. The manuscript delves into the methodologies for producing ZnO:B films, including reactive evaporation, evaporation from two sources, and flash evaporation, each addressing the challenges of achieving the desired film composition and structure. The investigation reveals that the optimized ZnO:B films possess crystalline phases with hexagonal lattice structures, demonstrating significant enhancements in electrical conductivity upon specific annealing treatments. The research underscores the impact of doping and microstructure modifications on the optoelectronic properties of ZnO films, contributing to advancements in semiconductor-based thin films and powders.

1 Introduction

Zinc oxide (ZnO) is recognized as a semiconductor with a direct wide bandgap (Eg ≈ 3.175 eV), rendering it a promising candidate for photonic and optoelectronic applications [1]. The significant excitonic energy (60 mV) of ZnO facilitates effective excitonic emission, which is advantageous for the development of ultraviolet light-emitting and laser diodes. Additionally, ZnO, in both its pure and doped forms, has been extensively studied for its potential in solar cells, photoelectrochemical cells (PECs), thin film transistors, gas sensors, and nanogenerators. The appeal of ZnO for these applications lies in its chemical and physical robustness, abundance, cost-effectiveness, and environmental compatibility. Furthermore, ZnO's bandgap and high optical transmittance make it suitable for use in organic and hybrid solar cells as a cathode buffer layer or transparent electrode. Crystalline ZnO demonstrates superior electrical properties in both bulk and thin film forms. Thin films, in particular, offer advantages such as reduced size, lightweight, stability, and versatility in configuration compared to bulk materials. Typically, undoped ZnO is rarely utilized; instead, the optoelectronic properties of ZnO are customized for specific applications through various

*Corresponding author: yusupov.fizika@gmail.com

processing techniques, including synthesis methods, doping mechanism optimization, introduction of impurities, microstructure control, and film thickness adjustment. Advancements in nanoscience and nanotechnology have driven the miniaturization and diversification of electronic and optical devices, prompting researchers to develop novel synthetic strategies for producing semiconductor-based thin films and powders on a practical scale [2]. ZnO films are especially valuable for transparent conductive layer applications in LEDs, flat panel displays (FPD), and solar cells, owing to their high transmittance in the visible region and commendable electrical conductivity [3]. The electrical properties of ZnO are linked to the presence of interstitial Zn atoms and crystal defects, such as oxygen vacancies resulting from non-stoichiometry and defects arising during grain growth. To enhance the conductivity of ZnO films beyond that of metallic films, various elements are introduced as impurities into the ZnO crystal lattice to replace Zn atoms. Elements from group III (B, Al, Ga, and In) and group IV (Ti, Zr, Sn, and Hf) are commonly employed to modify the properties of ZnO. The dopant efficiency is influenced by factors such as electronegativity and ionic radius. Another strategy involves modifying processing techniques to produce ZnO films with altered microstructures. The particle morphology, ranging from particles to tubes and wires in the nanometer or micrometer scale, and the surface morphology of films significantly impact the properties of the targeted devices.

2 Experimental methodology

The production of films containing boron (B) and borides poses technological challenges due to their high melting points, which hinder film formation via thermal methods. Moreover, their high electrical resistance complicates deposition processes such as cathode sputtering or electron bombardment. Consequently, films of various boron modifications and borides remain inadequately studied. The production of compound and alloy films demands a specialized approach because only a limited number of inorganic compounds, alloys, or mixtures can be evaporated without altering their composition. This is attributed to the different vapor pressures of the components in solid or liquid states, leading to a vapor composition that differs from the feed material's composition in the evaporator. Direct evaporation of materials for film deposition does not yield the desired results, necessitating the development of specialized methods such as reactive evaporation, evaporation from two sources, and the flash method. Despite each method having drawbacks, they are nearly the sole means for preparing films of complex compositions with practical significance.

Reactive evaporation, predominantly used for metal oxides, involves simultaneously directing metal vapor and an oxygen flow onto a substrate within a vacuum system. Film formation begins upon impact on the substrate, with the process controlled by the rates of metal atom and oxygen molecule arrival at the surface, the condensation coefficient, and the substrate temperature. However, reactive evaporation is unsuitable for producing films of dielectric material compounds.

Evaporation from two evaporators is commonly used for producing multilayer structures, employing two evaporators for different substances within the same vacuum system. Simultaneous operation allows the production of multi-component films that are unattainable via direct evaporation. Evaporating two materials at different temperatures and condensing them together eliminates fractionation and decomposition issues encountered with direct evaporation, enabling the production of films with desired compositions. However, controlling the condensation rates of film components, maintaining their proportions, and positioning evaporators to uniformly expose the substrate area to both vapor flows are key challenges.

Flash evaporation is employed for depositing films containing components with differing vapor pressures. This method involves continuously feeding small portions of evaporated

material components into the evaporator using specialized mechanical devices. A single evaporator is used, with a sufficiently high temperature to evaporate the least volatile substance.When using the flash method, the choice of material and design of the evaporator is of great importance, which must operate at temperatures of the order of 2000 ° C without evaporating the evaporator substance itself and not react strongly with the evaporated substance. In addition, the implementation of this method requires the solution of complex technical problems associated with the transportation of components of the original film material.

Of the methods described above, the last method would be most suitable for obtaining boride films. However, the installation of this method is very complex and the melting point of boron is very high (2200-2500°C). Therefore, in this work, based on the fact that, as noted by the authors of [4-14], red boron crystals, i.e. os - rhombohedral boron were grown at the eutectic temperature (830°C) in the Pt-B system, a special method was developed [1] for producing aluminum boride films by thermal evaporation in vacuum, based on the presence of the eutectic state in the MO_x-B system.

The essence of the method is that a thoroughly mixed powder mixture consisting of ZnO of technical purity and fine-crystalline or amorphous boron of 99.98% purity is placed in a tungsten crucible, pre-coated with aluminum oxide and reflected at temperatures of 1500 - 1600 ° C, heated up to a temperature of 1450°C in a vacuum not lower than 10-4 mmHg. Then if you open the curtain in front of him for 5-10 minutes. ZnO:B films of the required configuration and thickness of about 1 μm are formed on the surface of heated substrates made of glass, sapphire, silicon, copper, table salt and others.

The composition and crystal structure of the resulting films were subjected to thorough analysis, first at the Institute of Physics and Technology of the Russian Academy of Sciences and then at the International Center for Electron Microscopy (Halle, Germany) by senior researcher Yu.A. Shiyanov. using Auger spectroscopy and electron microscopy, respectively. The film composition is formed in the evaporator.

To determine the crystal structure, films sawn onto NaCl plates were used. The studies were carried out using a high-resolution electron microscope IEM-100C. The films were examined through transmission with magnification from 110 thousand to 1 million. Direct resolution of the crystal lattice was obtained using the two-beam method.

3 Results and discussion

Freshly sawn films in the initial state are amorphous. The electron diffraction pattern shows two highly blurred rings, characteristic of the amorphous phase (Fig.1). Heating the film directly in the column of an electron microscope with an electron beam leads to the appearance of clear narrow lines on the electron diffraction patterns (electron diffraction patterns 6OF6275 and 6OF6199), which indicates the appearance of a crystalline phase along with the amorphous phase (electron diffraction pattern).

Calculation of the electron diffraction pattern showed that the precipitated crystalline phase is an ZnO boride with a hexagonal lattice with periods α=7.835 Å, c=15.91 Å. The calculation results are shown in tables 1 and 2. [15-20].

These tables present data typically associated with the analysis of an electron diffraction pattern obtained from a crystalline material, in this case, a boron-doped Zinc Oxide (ZnO:B). Here's a breakdown of the table's columns: Diameter rings on electronogram (mm)- this column lists the measured diameters of the diffraction rings in millimeters as observed on the electronogram, which is an image or pattern obtained after electron diffraction. Ring intensity (produced units)- this column shows the relative intensity of each diffraction ring, which is often a measure of the number of electrons that have constructively interfered at that angle, indicative of the plane's atomic density. Measured d_{HKL} (Å)- this value represents the

interplanar spacing calculated from the diameter of the diffraction rings, using the Bragg's law equation. Tabular d_{HKL}: This column contains reference values for the interplanar spacings from established databases such as the American Society for Testing and Materials (ASTM). These are used to identify the material based on the diffraction pattern. Intensity (table 1 and 2.): this gives the relative intensity of the diffraction peaks as listed in standard reference materials, which can vary depending on the crystal's orientation, the presence of certain elements, and other factors. HKL ZnO:B: this represents the Miller indices (h, k, l) for the crystal planes that correspond to each ring. The Miller indices are a notation system in crystallography for planes in crystal (lattice) structures and are used to identify and describe the orientation of the planes. As can be seen from the tables 1 and 2, the experimental values of the lattice parameters agree quite well with the tabulated ones, which are taken from the ASTM file [12].

Table 1. Diameter rings on electronogram (mm)

Diameter rings on electronogram (mm)	Ring intensity (produced units)	Measured d_{HKL} (Å)	Tabular d_{HKL} (Å)	Intensity (table.)	HKL ZnO:B
8.8	5	5.26	5.27	50	003
14.4	3	3.20	3.18	100	113
17.8	3	2.60	2.60	10	024
19.2	2	2.41	2.39	10	122
22.0	3	2.10	2.08	35	303

Table 2. Ring diameter On the electron diffraction

Ring diameter On the electron diffraction	Ring intensity (produced units)	Measured dHKL (Å)	Tabular d_{HKL} (Å)	Intensity (table.)	HKL ZnO:B
9.0	1	5.27	5.27	50	003
15.0	1	3.17	3.18	100	113
18.8	3	2.53	2.54	20	211
25.6	3	1.90	2.02	40	125
28.0	5	1.32	1.37	15	224

Using the two-beam method, the early stages of crystallization of the amorphous film were photographed using a high-resolution microscope IEM-100C. The initial state of the film is shown in microphotograph (Fig.1.). Micrographs simulate an electron diffraction pattern of a crystalline film, which typically results from directing a beam of electrons at a thin slice of crystalline material. When electrons pass through the crystalline structure, they diffract according to the arrangement of atoms within the crystal, creating a pattern on a detector that reflects the crystal's symmetry and spacing of its lattice planes. The varying intensities of the spots correspond to the atomic planes from which electrons are diffracted. These diffraction patterns are key in determining the structure of crystals since they can provide information on the crystal lattice parameters, the orientation of the crystal, and any defects present within the material. Micrographs show dark-field images of the crystal lattices of boride ZnO:B type (012) with a period of 4.92 Å, with a magnification of 1 million times shows a snapshot of a ZnO:B microcrystal with a size of 200 Å, crystalline planes (012) with a period of 4.91 Å are visible.

In addition, dislocations in the form of extra half-planes are visible on it. Micrograph 110F6260 (Fig.2.) show bright-field images of ZnO:B crystallites after two hours of annealing. At this point, the crystallization process is completed, crystal grains of ZnO:B measuring 100 ÷ 300 Å are visible.

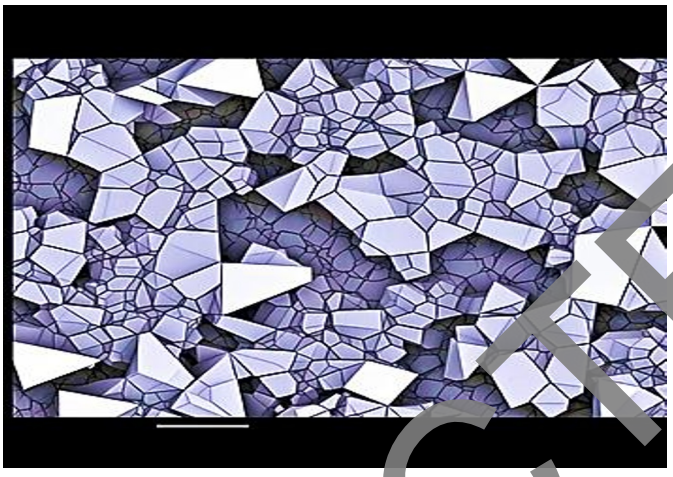

Fig.1. Electron diffraction pattern of a crystalline film.

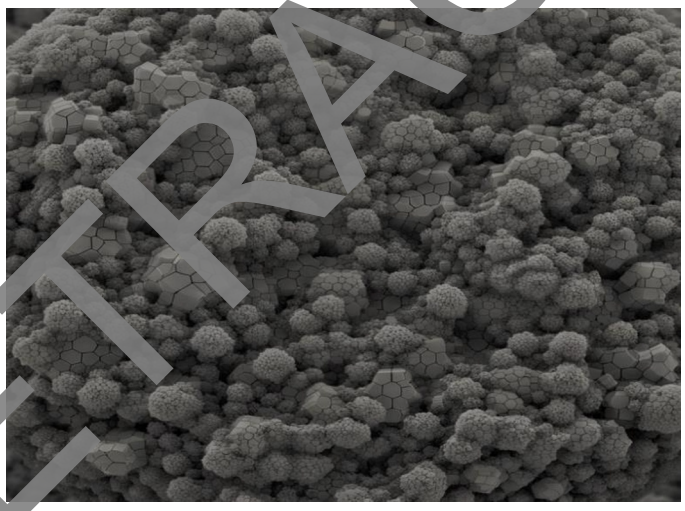

Fig.2. Bright-field images of ZnO:B crystals

The crystal lattices of grains are oriented in space in an arbitrary manner, in an ordered orientation, i.e. There is no texture in the film after crystallization. Electrical properties of amorphous and crystalline films of ZnO:B. Electrical measurements in the high temperature range were carried out on an installation created on the basis of an industrial vacuum installation VUP-5M. As noted above, the films were deposited onto substrates at different temperatures. Therefore, first of all, the connection between electrical conductivity and the temperature of the substrate and the annealing process was established.

The electrical conductivity of amorphous films decreases with increasing substrate temperature (Fig.3.). A similar effect is exerted by short-term annealing (up to 1 hour) at temperatures not exceeding the temperature of the substrate before film deposition.

Apparently this is caused by the fact that in both cases there is a decrease in the density of localized states in the mobility gap of the amorphous semiconductor. This is also evidenced by the increase in the parameter T_0 in the Mott formula, which describes conductivity at low temperatures with a variable jump length along localized states near the Fermi level. Thus, it can be argued that an increase in the substrate temperature and short-term annealing of films acts in the same way as is usually observed for amorphous (non-hydrogenated) semiconductors [21, 22].

At high temperatures, the slope of the straight lines $\sigma \sim f(T^{-1})$ is the same for all amorphous films. Therefore, assuming that in this case intrinsic conductivity occurs, the thermal band gap was calculated. It turned out to be equal to 1.2 eV. (Fig.4.). At least three hours of annealing at a temperature of 350 ÷ 400°C transforms all amorphous films into a crystalline state. In this case, the electrical conductivity decreases by approximately two orders of magnitude. The temperature dependences of electrical conductivity during the transition from amorphous to crystalline are shown in Fig.5.

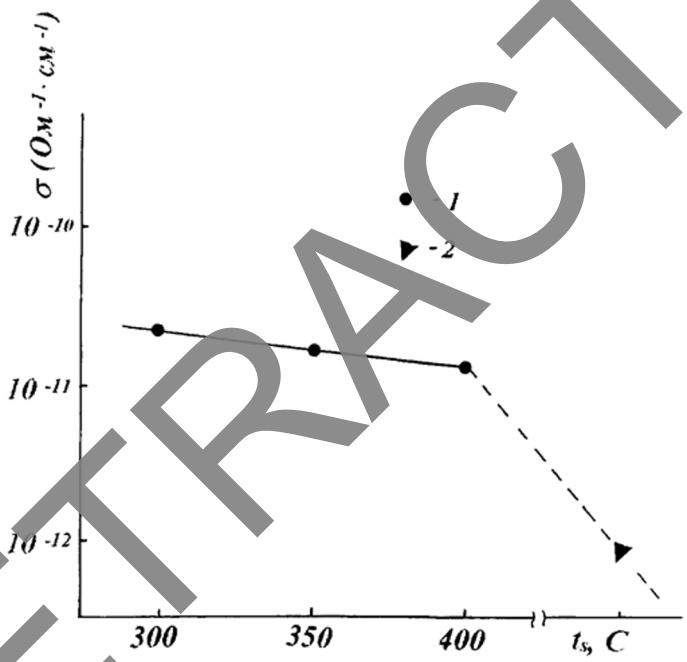

Fig.3. Dependence of the electrical conductivity of the ZnO:B film on the substrate temperature: 1-amorphous films; 2-crystalline films.

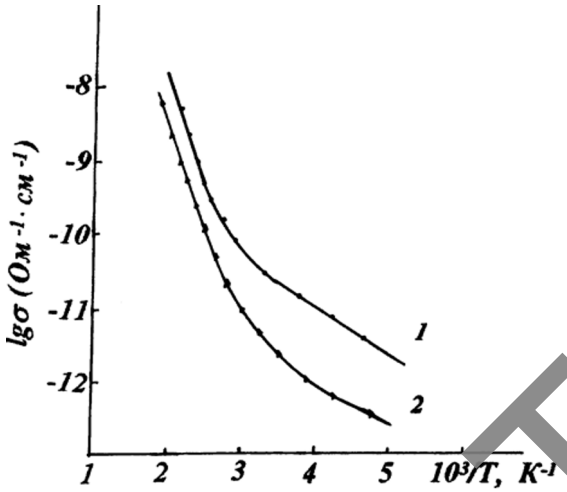

Fig.4. Temperature dependences of the electrical conductivity of amorphous ZnO:B films: 1 - without annealing; 2 - after three hours of annealing.

The temperature dependence and electrical conductivity value for all samples coincide within the measurement error.

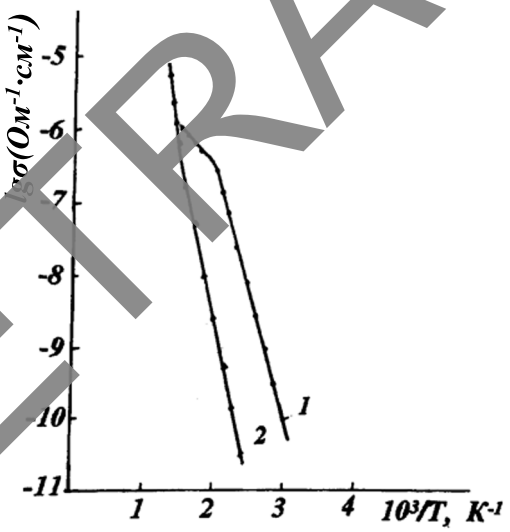

Fig.5. Temperature dependences of the electrical conductivity of amorphous (1) and crystalline (2) ZnO:B films.

An assessment of the thermal band gap in the high temperature region showed that it is equal to 1.8 eV. It follows that the temperature coefficient of resistance at room temperature is $B = -E/2\kappa = -4.3 \cdot 10^{-2}$ K^{-1} and lies within the TCS of industrial thermistors [14]. However, a thermistor made of ZnO:B will have a number of advantages: radiation resistance, chemical resistance, etc. Low-temperature measurements of the electrical conductivity of both

amorphous and crystalline films were carried out in the Laboratory of Semiconductor Device Physics of the Physicotechnical Institute of the Russian Academy of Sciences.The results obtained over a wide temperature range are presented in Fig.4. As can be seen from the figure, at low temperatures, crystalline films of ZnO:B exhibit hopping conductivity with a variable hopping length, characteristic of heavily doped and amorphous semiconductors. The dependences $\ln\sigma \sim (T_0/T)^{1/4}$ are presented in Fig.6. The T_0 parameter in Mott's law, calculated from this dependence, turned out to be equal to $8 \cdot 10^6$ K.

The thermal band gap Eg for hexagonal ZnO:B at room temperature is close to Eg α-AlB_{12}. However, the value of electrical conductivity σ_{300K} at room temperature for ZnO:B is several orders of magnitude lower.

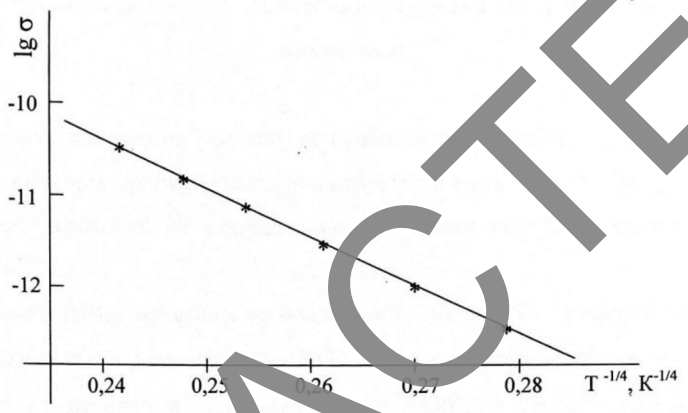

Fig.6. Dependence $1pst \sim (T_0/T)^{1/4}$

4 Conclusion

The study conclusively demonstrates that Zinc oxide (ZnO), when doped with boron (B) and subjected to optimized annealing processes, evolves from an amorphous state to exhibit a crystalline phase with a hexagonal lattice. This transition markedly improves the electrical properties of the films, making them suitable for a broad range of photonic and optoelectronic applications. The research highlights the effectiveness of various film production techniques, particularly reactive evaporation, for achieving desired compositional and structural outcomes in ZnO:B films. Furthermore, the findings contribute valuable insights into the role of doping and microstructural control in enhancing the optoelectronic characteristics of ZnO, paving the way for its application in advanced electronic and optical devices. The successful modification of ZnO films through doping and annealing underscores the material's versatility and potential in the fabrication of high-performance semiconductor devices.

References

1. Sultanov N., Mirzajonov Z., Yusupov F. (2023). E3S Web of Conferences, **458**, 01013. https://doi.org/10.1051/e3sconf/202345801013
2. Ahmed M.A., Coetsee L., Meyer W.E., Nel J.M. (2019). Journal of Alloys and Compounds, **810**, 151929. https://doi.org/10.1016/j.jallcom.2019.151929
3. Deng Y., et al. (2022). Nature Photonics, **16**, 505–511. https://doi.org/10.1038/s41566-022-00984-2

4. Won Y. H., et al. (2019). Nature, **575**, 634–638. https://doi.org/10.1038/s41586-019-1771-5
5. Ye J.D., et al. (2005). Journal of Crystal Growth, **283(3–4),** 279-285.
6. Kong B.H., et al. (2010). Thin Solid Films, **518(11),** 2975-2979.
7. Pietruszka R., et al. (2016). Solar Energy Materials and Solar Cells, **147**, 164-170.
8. Volkova M., Sondors R., Bugovecka L., Kons A., Avotina L., Andzane J. (2023). Scientific Reports, **13(1),** 21061. https://doi.org/10.1038/s41598-023-30019-x
9. Oday M., Abdulmunem, Mohammed J., Mohammed, Ali, Ehssan S., Hassan (2020). Optical Materials, **109**.
10. Awayssa O., Saevarsdottir G., Meirbekova R., Haarberg G. M. (2021). Journal of The Electrochemical Society, **168(4),** 046506. https://doi.org/10.1149/1945-7111/abf40e
11. Awayssa O., Haarberg G. M., Meirbekova R., Saevarsdottir G. (2021). Electrochemistry Communications, **125**, 106985. https://doi.org/10.1016/j.elecom.2021.106985
12. Parashar P.K., Kinnunen S.A., Sajavaara T., Toppari J., Komarala V.K. (2019). Solar Energy Materials and Solar Cells, **193**, 231-236. https://doi.org/10.1016/j.solmat.2019.01.019
13. Dulanto J., Fengler S., Sevillano-Bendezú M.A., Grieseler R., Guerra J.A., Töfflinger J.A., Dittrich Th. (2022). Thin Solid Films, **759**, 139474. https://doi.org/10.1016/j.tsf.2022.139474
14. Mahmood K., Abbasi S., Zahra R., Rehman U. (2018). Ceramics International, **44(15),** 17905-17908. https://doi.org/10.1016/j.ceramint.2018.06.263
15. Yigit E., Sevgili Ö., Bayindir S., Akman E., Orak İ., Dayan O. (2022). Materials Science and Engineering: B, **286**, 116036. https://doi.org/10.1016/j.mseb.2022.116036
16. Akhmadaliev, B.Z., Yuldashev, N.K. & Yulchiev, I.I. (2018). Opt. Spectrosc. **125**, 343–352. https://doi.org/10.1134/S0030400X18090023
17. Sevgili Ö. (2021). Solid State Sciences, **117**, 106635. https://doi.org/10.1016/j.solidstatesciences.2021.106635
18. Yiğit E., Sevgili Ö., Orak İ. (2023). Applied Physics A, **129**, 194. https://doi.org/10.1007/s00339-023-06432-4
19. Akhmadaliev, B.Z., Yuldashev, N.K. (2021). Opt. Spectrosc. **129**, 1187–1192. https://doi.org/10.1134/S0030400X21090022
20. Turut A., Karabulut A., Efeoğlu H. (2021). Journal of Materials Science: Materials in Electronics, **32**, 22680–22688. https://doi.org/10.1007/s10854-021-06753-1
21. Ashery A., Elnasharty M.M.M., Hameed T.A. (2020). Optical and Quantum Electronics, **52**, 490. https://doi.org/10.1007/s11082-020-02601-4
22. Tanrıkulu E.E., Altındal S., Yerişkin S. (2021). Physica B: Condensed Matter, **623**, 413345.